Spontaneous-emission coupling factor and mode characteristics of planar dielectric microcavity lasers

Gunnar Björk
Department of Microwave Engineering, Royal Institute of Technology, Box 700 33, S-100 44 Stockholm, Sweden

Henrich Heitmann and Yoshihisa Yamamoto
NTT Physical Science Research Laboratories, 3-9-11 Midori-cho, Musashino-shi, Tokyo 180, Japan
(Received 8 September 1992)

The spontaneous-emission coupling factor β for planar microcavities without lateral confinement is measured and calculated for gain media with finite spontaneous-emission linewidth. It is shown that in order to maximize β, the spontaneous-emission linewidth of the gain medium must be smaller or equal to the cold-cavity linewidth. It is also shown that the planar-cavity geometry will give rise to spatial modes, and in order to maximize β one should pump only an area corresponding to one spatial mode. If the pumped area is larger than the lateral extent of a cavity mode, then the mode will grow laterally when pumped above threshold.

PACS number(s): 42.55.Px, 42.50.Lc

I. INTRODUCTION

Lasers with cavity volumes on the order of one wavelength cubed are commonly referred to as microcavity lasers. In these small lasers the mode density per unit frequency is small, and consequently the threshold pump power will also be small, since spontaneous emission into the nonlasing modes usually constitutes the largest dissipation of pump power below threshold [1, 2]. It has been predicted that threshold pump powers below 1 μW should be possible using semiconductor material [3, 4], and a few μW threshold pump powers have been reported [5,6]. Hence microcavity lasers hold great promise for the future.

Recently, many different microcavity geometries have been proposed, such as planar, post [7], disk [5], droplet [8], and hemispherical cavities [9]. The simplest of the cavities from the viewpoint of semiconductor fabrication technology may be the planar dielectric Bragg-mirror cavity. However, in an earlier paper [10] we have pointed out that in contrast to laterally confined cavities such as post, disk, and droplet cavities, the maximum achievable spontaneous-emission coupling factor in a planar cavity is limited by the refractive indices in the Bragg stack. In our earlier analysis we assumed a spontaneous-emission linewidth much smaller than the cold-cavity linewidth. In this paper the analysis is generalized, and it is shown that if the spontaneous-emission linewidth is broader than the cold-cavity linewidth, β is decreased by a factor equal to the ratio between the linewidths. This is a general result pertaining to most microcavity geometries. Specifically, it has already been shown that this is also the case for dielectric post lasers [11] and hemispherical lasers, and it will be a difficult obstacle to overcome in the pursuit of low-threshold microcavity lasers operated at room temperature.

A difficulty with the planar dielectric cavity is that, since there is no lateral confinement of the mode, the transverse modes of the cavity have been poorly defined, and, consequently, so has β. In this paper we will show that modes can be relatively well defined, but they will be localized spatially. Whereas every mode in a perfect cavity with lateral confinement will occupy the whole cavity, the modes of the nonperfect laterally unguiding planar cavity will be spatially localized in the cavity. In some sense it can be said that the modes themselves define the cavity. Moreover, above threshold, the lateral extent of the modes will grow, and finally only one (or rather two) mode will fill the whole pumped area. This can be viewed either as locking of all the spatial modes within the pumped area to a coherent supermode, or as growth of the spatial mode due to decreased effective cavity loss. When the spatial mode grows, the divergence angle of the emitted radiation narrows. The divergence angle narrowing can be shown to be in complete analogy with the narrowing of the laser linewidth above threshold.

The paper is organized as follows. In Sec. II the spontaneous-emission intensity from a planar dielectric cavity is calculated. Analyzing the emission pattern it is possible to define cavity modes and to calculate how much of the total emission is emitted into this mode. In Sec. III we compare the behavior of the spontaneous-emission coupling factor and the number of cavity modes of the planar cavity with that of a laterally guided cavity. In Sec. IV we show that planar dielectric cavities potentially may be suitable for relatively high-power, low-divergence-angle lasers due to the lateral spread of the mode above threshold. In Sec. V we review some experimental results and compare with the theory in the previous sections. In Sec. VI some of our conclusions are summarized.

II. SPONTANEOUS EMISSION IN PLANAR DIELECTRIC CAVITIES

A. Spontaneous-emission intensity

The model of the planar dielectric Bragg-mirror cavity used in the paper is depicted in Fig. 1. The cavity is

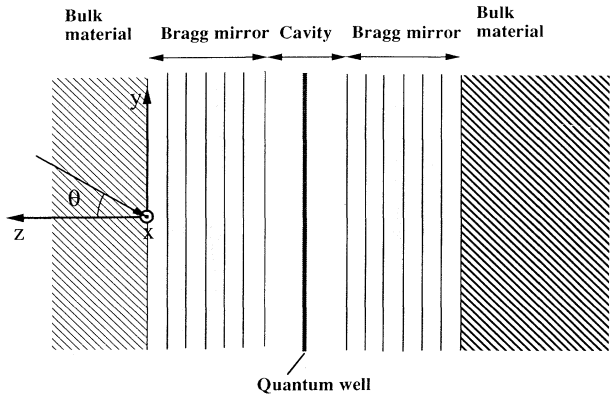

FIG. 1. Cross section through a planar dielectric cavity.

assumed to extend to infinity in both of the lateral directions (x and y), and it is assumed to be surrounded by isotropic and homogeneous bulk dielectric media extending to infinity in all three directions. In practice, the surrounding media are often different, e.g., air on one side and semiconductor substrate material on the other. The cavity consists of a dielectric slab, one wavelength thick, in which a thin sheet of active material (in practice this is a quantum well) is embedded. The dielectric slab is sandwiched between two dielectric Bragg mirrors each consisting of $2M$ layers of alternating high- and low-refractive-index dielectric slabs (M slab pairs). The z axis is normal to the cavity plane, and the incidence angle θ is defined as shown in the figure.

To calculate the spontaneous emission emitted from a planar cavity we use the technique described in [10]. The propagating vacuum fields incident on the cavity from the surrounding bulk material are expanded in an orthogonal plane-wave basis. The modification of the planar-wave-mode functions at the location of the active material due to multiple-reflection interference is computed by the use of a transfer-matrix method (evaluated numerically), and the spontaneous emission emitted into the mode is assumed to be proportional to the absolute square of the mode modification factor. Four such modification factors must be computed, as, in general, they are different for p and s polarization, and they are different for the vacuum fields impinging on the left- and right-hand side. In addition, if the surrounding bulk media are different, one must take into account that the mode densities and electric-field rms expectation values are different for the vacuum fields impinging from the right- and left-hand sides. Furthermore, the orientation of the active-material dipole moment must be considered, as it is often not isotropic in thin quantum wells. Finally, to evaluate the spontaneous emission per unit solid angle and unit wavelength, one must weigh the (absolute square of the) modification factors with the bulk material spontaneous emission per unit wavelength, that is, the line shape of the spontaneous emission when unperturbed by cavity mirrors. The theory behind the method is described in some detail in [10] and will not be repeated here.

The calculated far-field spontaneous emission per unit solid angle and unit wavelength of a planar dielectric cavity with its active material dipole moment oriented in the xy plane is shown in Fig. 2. To separate the influence of the cavity on the spontaneous emission from the influence of the bulk spontaneous-emission line shape, the latter was assumed to be a constant, independent of wavelength. In order to simulate one of our fabricated samples [6], we have used the following cavity data. The active medium was a GaAs quantum well with a homogeneously broadened emission peak at 786 nm. The one-wavelength-long cavity was fabricated in $Al_{0.3}Ga_{0.7}As$ ($n \approx 3.47$ at 786 nm). The surrounding Bragg mirrors were made from alternating layers of AlAs ($n \approx 3.08$) and $Al_{0.15}Ga_{0.85}As$ ($n \approx 3.6$). The Bragg mirrors, with

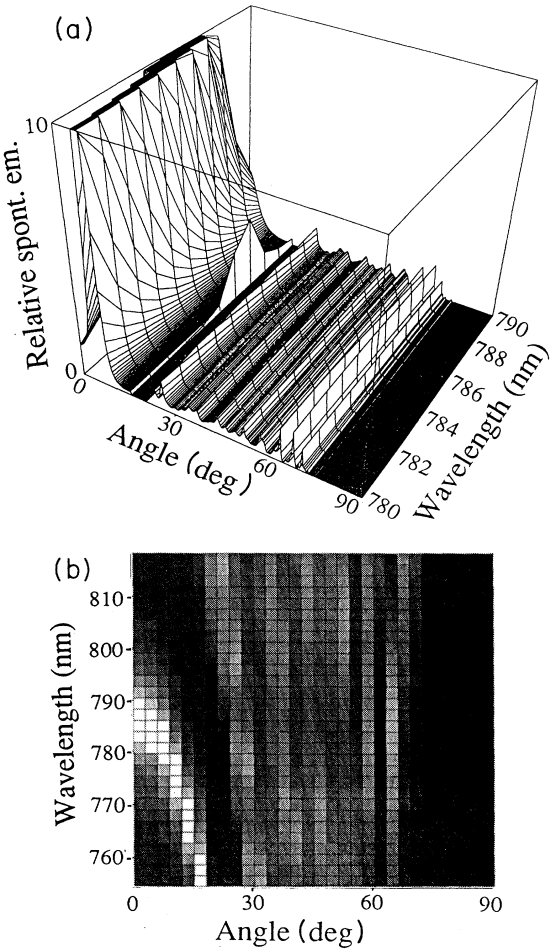

FIG. 2. Computed spontaneous emission per unit solid angle and unit wavelength (arbitrary units) vs emission wavelength and propagation angle in the cavity. The z axis in (a) has been truncated at about one-fourth of the spontaneous-emission maximum to resolve details in the passband. In (b) a density plot over the spontaneous-emission intensity has been drawn. White represents values > 2.5 in. [cf. (a)], black represents zero. It can be seen that the spontaneous emission has its maxima on a half parabola on the lower wavelength side. The jaggedness in both figures is due to the limited plot resolution.

a Bragg wavelength of 786 nm, were surrounded by bulk GaAs on one side ($n \approx 3.65$) and air on the other side.

On the air side the Bragg mirror of the fabricated sample consisted of 23 layer pairs, on the substrate side the number of layer pairs was 29.5. This yielded almost identical calculated reflectivities (as seen from the cavity) of 99.91% and 99.94%, respectively. The calculated photon lifetime was 5 ps. From the cavity-transmission measurements, and far-field lobe angle measurements presented in Sec. V, we deduced that the reflectivities were lower in the real sample. The reason for this shorter lifetime is not clear, but is most likely the combination of non-radiative absorption in the Bragg mirrors or quantum well and less than perfect control over mirror layer thicknesses.

In Fig. 2, which is drawn assuming 9 slab pairs in the air-side Bragg mirror and 13 slab pairs in the substrate Bragg mirror for demonstration purposes (the corresponding plot for the 23- and 29-pair laser spans over about four orders of magnitude and has only a 0.065-nm-wide resonance peak), it can be seen that at angles between 70° and 90° there will be very little spontaneous emission. This is because at angles greater than $\arcsin(3.08/3.47) \approx 62°$ the vacuum fields impinging from the GaAs substrate will be evanescent in the AlAs Bragg-mirror layers and will decay approximately exponentially as a function of distance from the surface in the GaAs side Bragg mirror. However, at certain angles the evanescent waves will tunnel resonantly through the structure. Three such resonant evanescent tunneling peaks can be seen between 62° and 70° in the figure. At slightly smaller angles (between 20° and 60°) the Bragg-mirror reflectivity is low since the Bragg wavelength of the mirrors as seen from these angles does not match the emission wavelength. Hence the sample is more or less transparent, it will have a passband, and the spontaneous emission per unit solid angle and unit wavelength will be very nearly the same as if no mirrors were present. There will only be a small but rapid modulation due to the Bragg mirrors. At smaller angles still (10°– 20°) the emitted radiation is very small. The reason is that the mirror reflectivity at these angles is high, but the cavity is out of resonance (the phase condition is not met). The incident vacuum fields are simply reflected back and cannot penetrate the cavity. In our earlier paper we called this the stopband. It can be seen that the stopband is almost wavelength independent. [The narrow peak around $\arcsin(1/3.47) \approx 16.7°$ and 786 nm is due to the cutoff of the vacuum fields impinging from the air side. It too is relatively wavelength independent, but as a consequence of limited plot resolution and a very narrow peak, it looks like it exists only around 786 nm.]

Finally, near normal propagation angles, and at wavelengths equal to or shorter than the resonant wavelength, the spontaneous emission per unit solid angle is largest. Since the (complex) amplitude reflectivity of a Bragg mirror is real where its reflectivity is highest (around the Bragg wavelength), the cavity resonance condition for an incident plane wave can simply be written

$$\exp(j2k_z L_{\text{cav}}) = 1 \quad , \tag{1}$$

where k_z is the z component of the plane-wave k vector, and L_{cav} is the cavity-dielectric-slab thickness. Re-expressing k_z in cavity wavelength and incident angle in the cavity, $k_z = 2\pi\cos(\theta)/\lambda$, and assuming that the resonant wavelength for $\theta = 0$ is $\lambda_r(0)$, the resonant wavelength for an arbitrary incidence angle becomes

$$\lambda_r(\theta) = \lambda_r(0)\cos(\theta) \quad . \tag{2}$$

For small angles θ, Taylor expansion of this formula yields

$$\Delta\lambda = \lambda_r(0) - \lambda_r(\theta) \approx \lambda_r(0)\,\theta^2/2 \quad . \tag{3}$$

Finally, expressing (3) in vacuum wavelength λ_0 and incident angle in vacuum θ_0, one gets

$$\Delta\lambda_0 \approx \lambda_{r0}(0)\theta_0^2/(2n_{\text{cav}}^2) \quad , \tag{4}$$

where n_{cav} represents the cavity refractive index, and Snell's law has been used. The manifestation of (4) can easily be seen in Fig. 2. The spontaneous-emission peak extends along a ridge in a half parabola on the lower-wavelength side in Fig. 2. If the emission wavelength is smaller than the cavity resonant wavelength, the maximum spontaneous emission per solid angle will no longer be in the direction perpendicular to cavity plane [12], but at an angle given by (4).

In deriving Eqs. (1)–(4) it has been assumed that the reflection phase of the Bragg mirrors are independent of θ (always real). This is essentially true for small angles and for wavelengths near the Bragg wavelength. In fact, for a given Bragg mirror, the reflectivity can be expressed explicitly in k_z and θ only, and it depends only very weakly on the latter around normal incidence. Hence, for the cavities considered in this paper, which have high mirror reflectivity and are designed to be resonant at normal incidence around the Bragg wavelength, the resonance characteristics is governed only by k_z. Thus a change of k_z by changing the incidence angle by a (small) amount θ_0 from the normal direction, keeping the wavelength constant, will change the resonance condition (and the mode modification function and consequently the spontaneous-emission rate into the plane-wave mode) by the same amount as a change of wavelength by the amount prescribed by (4) at normal incidence. This is a very useful result, and we will base our mode definition on this observation.

From Fig. 2 it can be deduced that if the spontaneous-emission linewidth is small compared to the cold-cavity resonance linewidth, the resonant mode will occupy a well-defined solid angle. In an earlier paper [10] we defined the mode as extending in angle from the normal direction to the angle at the first spontaneous-emission minima (close to the center of the stopband). In this paper we will be a little bit more conservative and define the angular extension of the mode to the full width at half maximum (FWHM) of the spontaneous emission per unit solid angle and unit wavelength central peak. In reality the difference between the two mode definitions mean little, since only a small amount of the spontaneous emission is emitted between the FWHM and the first minima.

It is relatively easy to show that the FWHM in wavelength of the spontaneous emission is identical with the

FWHM of the cavity transmittivity, if the gain medium is located at the center of the cavity. The FWHM of the transmittivity expressed in wavelength can be computed easily as a function of the mirror reflectivities R_1 and R_2, the resonance wavelength, and the cavity length. The transmittivity of the planar cavity is

$$T = \frac{\sqrt{(1-R_1)(1-R_2)}}{1-\sqrt{R_1R_2}\exp(j2k_zL_{\text{cav}})} \quad . \tag{5}$$

It is straightforward to derive the FWHM of T. Expressed in k_z it is

$$\Delta k_{z,\text{FWHM}} = \frac{1-\sqrt{R_1R_2}}{L_{\text{cav}}(R_1R_2)^{1/4}} \quad . \tag{6}$$

This corresponds to a spread in vacuum wavelength of

$$\Delta\lambda_{\text{FWHM0}} = \frac{\lambda_{r0}^2}{2\pi L_{\text{cav}}n_{\text{cav}}}\frac{1-\sqrt{R_1R_2}}{(R_1R_2)^{1/4}} \quad . \tag{7}$$

Using (4) above, the spread in incidence angle at $\lambda_0 = \lambda_{r0}$ can similarly be expressed

$$\Delta\theta_{\text{FWHM0}} = \sqrt{\frac{2\lambda_{r0}n_{\text{cav}}}{\pi L_{\text{cav}}}\frac{1-\sqrt{R_1R_2}}{(R_1R_2)^{1/4}}} \quad . \tag{8}$$

In Fig. 3(a) the spontaneous emission per unit solid angle and unit wavelength at the resonant wavelength λ_{r0} is drawn versus the propagation angle in the cavity. The FWHM is about 6.0°, corresponding to a $\Delta\theta_{\text{FWHM0}}$ in vacuum (air) of 21.0°. In Fig. 3(b) the same quantity is plotted versus wavelength at normal incidence. The FWHM in the figure corresponds well to the value predicted by inserting (8) in (7) of 2.2 nm. It should be noted that (7) and (8) were derived using a lumped mirror model whereas Fig. 3 was computed using the distributed Bragg-mirror model. The less exact lumped model thus works well near normal incidence, provided that one uses the effective cavity length. In this case, where the computed mirror reflectivities (as seen from the cavity) were 93% each, the effective cavity length can be computed to be 918.7 nm from (8). This should be compared to the 226.5-nm length of the "cavity" dielectric slab. The effective cavity thus extends a few slab pairs into each Bragg mirror.

B. Cavity spatial modes

The well-defined angular half-width of the mode $\Delta\theta_{\text{FWHM0}}$ indicates that the mode is also well confined spatially. The isotropy in the xy plane of planar cavities dictates that the mode can be defined by its radius a_p. Using classical divergence theory we find that the far-field intensity I from a uniformly illuminated circular aperture is given by Airy's formula

$$I(\theta) = \left[\frac{2J_1[ka\sin(\theta)]}{ka\sin(\theta)}\right]^2 I_0 \quad , \tag{9}$$

where $I(0) = I_0$ and J_1 denotes the first Bessel function of the first kind. Replacing $ka\sin(\theta)$ by x and noting that the equation $8J_1^2(x) = x^2$ is approximately solved for $x = 1.5$, the half-width at half maximum (HWHM) of the intensity function gives

$$a_p \approx \frac{1.5}{k\sin(\theta_{\text{HWHM}})} \approx \frac{\lambda}{2\theta_{\text{FWHM}}}. \tag{10}$$

Using (8) we can express the mode radius in cavity parameters as

$$a_p \approx \sqrt{\frac{\pi\lambda_{r0}L_{\text{cav}}}{8n_{\text{cav}}}\frac{(R_1R_2)^{1/4}}{1-(R_1R_2)^{1/2}}} \approx \sqrt{\frac{\pi\lambda_{r0}L_{\text{cav}}}{8n_{\text{cav}}[1-(R_1R_2)^{1/2}]}} \quad , \tag{11}$$

where $R_1, R_2 \approx 1$ has been assumed in the last step.

This result can be derived in a more strict sense if we consider the limiting case where we want to know how many modes there are in a microcavity with fixed length, within an area A, in a certain frequency interval around the resonant frequency. Since the longitudinal-mode spacing in a microcavity laser is very large, and the cavity length is assumed to be fixed, we need only to consider the transverse mode density. The transverse-mode density per unit frequency ρ can be written

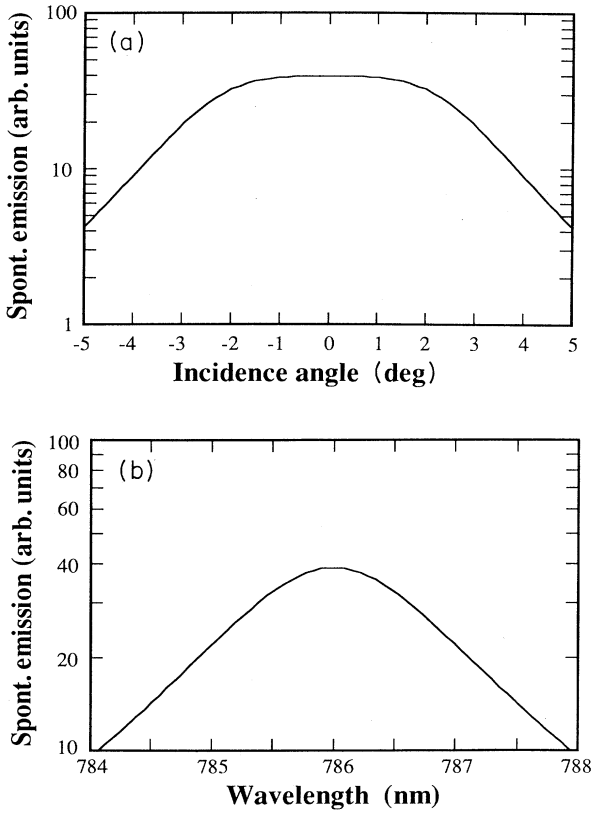

FIG. 3. The computed spontaneous emission vs the propagation angle (in the cavity) at the resonant wavelength in (a), and vs the wavelength ($\theta = 0$) in (b). The cavity parameters are the same as in Fig. 2.

$$\rho(\nu) = \frac{4\pi n_{\rm cav}^2 \nu A}{c_0^2} \quad . \tag{12}$$

The frequency interval within which the modes lie is given by (6), which can be translated to frequency by $\Delta\nu = c_0\Delta k/(2\pi n_{\rm cav})$. The number of transverse modes within the cavity bandwidth is thus

$$\frac{2n_{\rm cav}A(1-\sqrt{R_1R_2})}{\lambda_0 L_{\rm cav}(R_1R_2)^{1/4}} = \frac{2A}{\pi\dfrac{\lambda_0 L_{\rm cav}(R_1R_2)^{1/4}}{\pi n_{\rm cav}(1-\sqrt{R_1R_2})}} \quad . \tag{13}$$

Pumping an area A much larger than πa_p^2, a number $2A/\pi a^2$ of spatial modes will form (the factor of 2 accounts for polarization degeneracy). Identification with (13) immediately gives us the expression for the mode radius

$$a_p = \sqrt{\frac{\lambda_{r0}L_{\rm cav}(R_1R_2)^{1/4}}{\pi n_{\rm cav}[1-(R_1R_2)^{1/2}]}} \approx \sqrt{\frac{\lambda_{r0}L_{\rm cav}}{\pi n_{\rm cav}[1-(R_1R_2)^{1/2}]}} \quad . \tag{14}$$

This result is identical to (11), to within a small numerical factor. However, since (13) has been more rigorously derived, we will base our definition of the mode radius on it. It also corresponds to the result derived by Ujihara [13] to within a numerical factor of order unity. Moreover, it is consistent with the observation by De Martini, Marrocco, and Murra [14] that the spontaneous emission from two laterally separated points in a planar cavity is only correlated within a distance proportional to $[1-(R_1R_2)^{1/2}]^{-1/2}$. It can also be derived from Heisenberg's uncertainty principle for position and momentum. At a given emission wavelength, the uncertainty (or spread) in k_z will lead to an uncertainty in transverse momentum (say, in the x direction). This will lead to an uncertainty (spread) in lateral (e.g., x) position. The result from such a calculation again agrees with (14) to within a numerical factor of order unity.

The result that even in a planar-cavity geometry, relatively well-defined cavity modes are formed, allows us to understand how the planar cavity works. Pumping an area A much larger than πa_p^2, a number $2A/\pi a_p^2$ of spatial modes will form. As all the spatial modes are mutually incoherent, the far-field pattern of the superposition of the spontaneous emission emitted from each mode, as a function of wavelength and angle, will remain the same as that from a single spatial mode. Even if the pumped area is much smaller than the lateral spread of one spatial mode, the spontaneous-emission intensity distribution will remain the same, provided that net quantum-well (QW) absorption in the unpumped mode region is negligible compared to mirror losses.

In the discussion above we have been somewhat casual in our definition of cavity modes. We have, e.g., implicitly assumed that the number of modes can take on noninteger values. In reality, the boundary conditions of the specific cavity and pump configuration will uniquely determine the modes in that particular setup. However, the details are often not important for our purposes, since a typical planar dielectric cavity emits most of its spontaneous emission into radiation continuum modes (the emission between 20° and 90° in Fig. 2) which are difficult to handle as strictly quantized modes anyhow. Therefore, with the derivations above we will move on and calculate the spontaneous-emission coupling factor of the planar cavity.

C. Spontaneous-emission coupling factor

The spontaneous-emission coupling factor of a mode is defined as the ratio between the spontaneous-emission radiated into the mode and the total spontaneous-emission radiated by the atom system. It is important to realize that β is the result of the interaction between the cavity and the radiating system. Hence β depend as much on the radiating system as on the cavity. The same cavity will in general have different spontaneous-emission coupling ratios depending on what radiating system is put in them.

In our case we have assumed that the GaAs quantum-well excitonic system has its dipole moment oriented in the xy plane and that the emission line is homogeneously broadened. We furthermore assume that the excitonic-polarization-decay time is much faster than the cavity-photon lifetime.

For such a system the spontaneous emission per unit solid angle and unit wavelength at a certain direction and wavelength can be computed as explained above. In Fig. 4 the spontaneous emission emitted per unit solid angle and unit wavelength (arbitrary units) has been drawn, assuming a Gaussian material

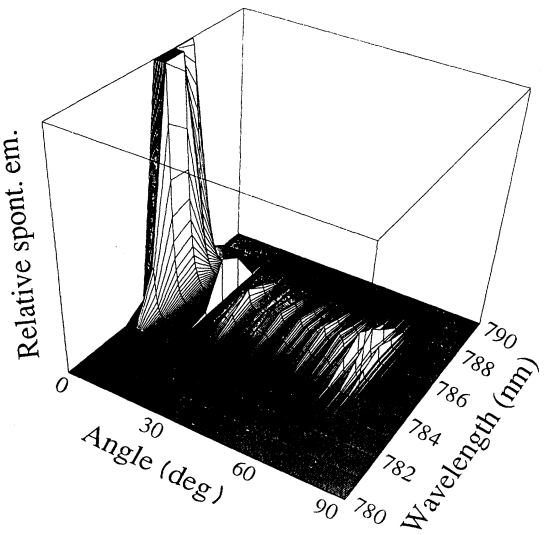

FIG. 4. The computed spontaneous emission per unit solid angle and unit wavelength as a function of angle (in the cavity) and wavelength is shown. The gain linewidth has been assumed to be 2 nm, slightly smaller than the cold-cavity linewidth of 2.2 nm.

gain function with a FWHM of 2 nm, slightly smaller than the cold-cavity linewidth of 2.2 nm. From the Fig. 4 and the underlying model it can be deduced that the emission into the mode has both its electric and magnetic field in the xy plane. The cavity resonant mode thus resembles a TEM_{00} Gaussian mode.

The spontaneous-emission coupling factor can be calculated by integrating the spontaneous emission into one of the polarization directions per unit solid angle and unit wavelength over the solid angle of the mode and over the cold-cavity bandwidth and dividing by the same integral over both polarizations, all solid angle and all wavelengths. In Fig. 4 all radiation is accounted for, both the s and p polarized. Since the active material in our case has its dipole moment oriented in the xy plane, the radiation propagating close to the z axis belongs to an equal superposition of the two orthogonally polarized modes. Hence β can be calculated relatively easily by integrating the function in Fig. 4 within the mode-definition angle and wavelength range, dividing the integral by 2, and dividing again by the same integral taken over all solid angle and all wavelengths.

From Figs. 2 and 4 it is easy to be mislead into believing that most of the spontaneous emission is emitted into the resonant mode. This is incorrect. In fact, only a few percent of the total spontaneous emission goes there. Although the spontaneous emission per unit solid angle is much larger at the resonance near the normal direction than in the passband, very little solid angle is available in the normal direction. Since the total spontaneous emission is the integral over all solid angle, and the solid angle available as a function of θ is proportional to $\sin(\theta)$, it turns out that it is the spontaneous emission emitted in the passband (between 20° to 60° in Figs. 2 and 4) that, by far, carries away most of the emitted radiation. This is a problem inherent to all planar dielectric cavities.

In Fig. 5, the spontaneous-emission coupling factor as a function of the linewidth ratio $\Delta\lambda_{em}/\Delta\lambda_{FWHM0}$, where $\Delta\lambda_{em}$ is the FWHM of the material gain function, has been calculated by numerical integration for three different cavities. The atomic gain function has been assumed to be Gaussian, centered on the cavity resonance wavelength. Since β is relatively insensitive to the exact shape of the gain function (it is mainly sensitive to the width of the function), this should be a good approximation of the real situation. The cavities have been assumed similar to that in Fig. 2, except that the number of slab pairs in the Bragg mirrors has been used as a parameter. The three curves are very similar. The difference is comparable to the truncation errors in the (two-dimensional) numerical integration of the spontaneous emission. In fact, we believe that in absence of numerical truncation errors, the curves would be identical. When doing the truncation, care has been taken to keep the relative and not the absolute truncation error constant at every point.

From Fig. 5 it is clear that the optimum β is independent of the number M of slab pairs in the Bragg mirrors. We have shown earlier [10] that for symmetric cavities (equal Bragg mirror reflectivity) β depends only on the refractive indices of the Bragg mirrors and the cavity.

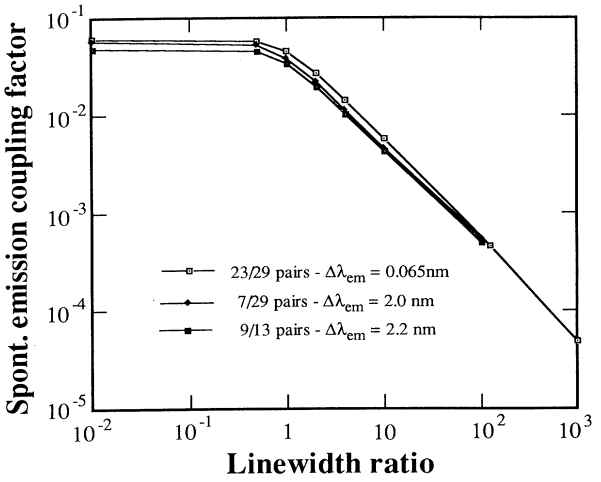

FIG. 5. The spontaneous-emission coupling factor as a function of the relative linewidth $\Delta\lambda_{em}/\Delta\lambda_{FWHM0}$. The cavity data are the same as in Fig. 2, but the number of mirror pairs have been assumed to be 23 and 29 (symmetric cavity, 0.065-nm cold-cavity linewidth), 7 and 29 pairs (asymmetric cavity, 2.0-nm linewidth), and 9 and 13 pairs (symmetric cavity, 2.2-nm linewidth).

When the FWHM of the gain function $\Delta\lambda_{em}$ is substantially narrower than the cold-cavity linewidth $\Delta\lambda_{FWHM0}$; the calculated β is around 0.055.

If $\Delta\lambda_{em}$ is larger than $\Delta\lambda_{FWHM0}$, β is rapidly degraded, as manifested by Fig. 5. Spontaneous emission will be emitted at wavelengths not belonging to the cavity mode, and most of it will be emitted at angles where the Bragg mirrors are transparent and independent of wavelength. Thus the spontaneous emission in the passband will increase linearly with $\Delta\lambda_{em}$ and β will decrease linearly.

The general behavior in Fig. 5 follows that calculated for dielectric post cavities [11] and hemispherical cavities [9]. β remains high and constant as long as $\Delta\lambda_{em}$ is smaller than $\Delta\lambda_{FWHM0}$, but as soon as $\Delta\lambda_{FWHM0}$ is smaller than $\Delta\lambda_{em}$, β starts to drop proportionally to the ratio of the half-widths. The conclusion is that, unless there is a forbidden gap in all spatial directions centered around the cavity resonance (as in a photonic band-gap structure [15]), *the atomic-gain linewidth must be narrower than the cold-cavity linewidth* to realize the optimum β. This will be a major obstacle to overcome since the cavity loss per pass cannot exceed the QW gain per pass if the structure is to lase. Since the latter is of the order 1% per pass, the mirror reflectivity must be of the order 99%. For a half-wavelength-long cavity emitting at 1-μm wavelength, a gain linewidth smaller than or equal to 0.3 nm is required to fulfill this condition. The two solutions employed so far to solve this problem have been utilization of multiple quantum wells to relax the high-mirror-reflectivity requirement and the use of excitonic resonances in combination with cooling [6,16] to reduce thermal-gain linewidth broadening.

An important thing to keep in mind when doing measurements on planar microcavities is to use proper filter-

ing when trying to measure $\Delta\lambda_{\mathrm{FWHM0}}$, $\Delta\theta_{\mathrm{FWHM0}}$, or β. When measuring $\Delta\lambda_{\mathrm{FWHM0}}$ by, e.g., measuring the cavity transmittivity (in practice this is done by measuring the cavity reflectivity), it is important to filter the reflected light angularly, so that only light close to normal incidence is collected. If not, it is easy to overestimate $\Delta\lambda_{\mathrm{FWHM0}}$ because of the resonance "ridge" on the lower wavelength side of the resonant wavelength in Fig. 2.

In Fig. 6(a), the spontaneous emission per unit solid angle is plotted versus the propagation angle in the cavity. The emission has been integrated over all wavelengths, and a gain linewidth of 20 nm has been assumed. This corresponds to an unfiltered measurement. It is seen that the central lobe has a FWHM of 18°, three times the actual FWHM of the cavity. From this figure (which should be compared to Fig. 3) it is obvious that if one tries to estimate $\Delta\lambda_{\mathrm{FWHM0}}$ from a lobe angle measurement, it is important to filter the light (which presumably is broadband spontaneous emission or reflected white light) in a narrow interval around the resonance wavelength. Otherwise, the measurement will be corrupted by the resonance ridge.

Collecting all light within the apparent 18° mode lobe angle, the spontaneous emission per unit wavelength will have a broadened and distorted look shown in Fig. 6(b). Since little angular filtering was undertaken (only the emission in the passband was not included), the linewidth appears broader than it really is. Proper spatial filtering would have eliminated the emission on the short wavelength side which does not belong to the cavity mode.

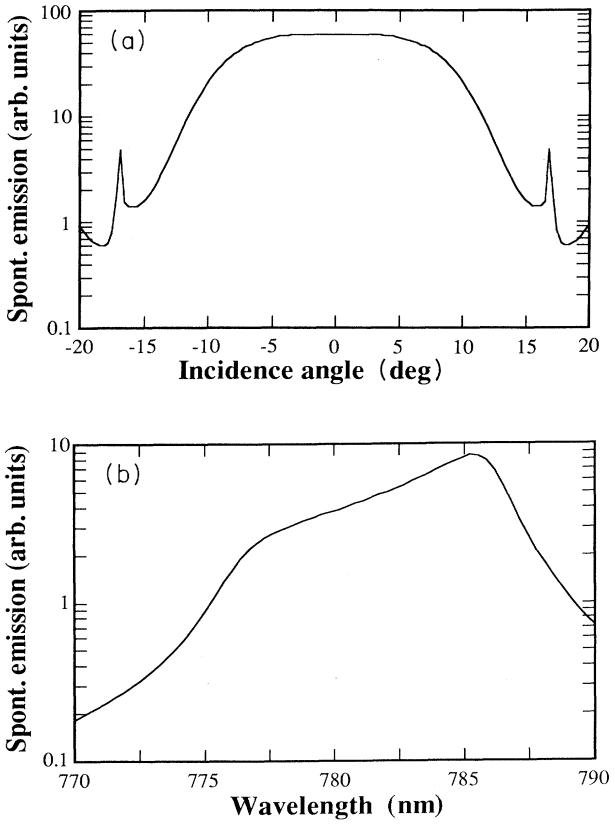

FIG. 6. (a) The computed spontaneous emission per solid angle vs the propagation angle (in the cavity) using no wavelength filtering. (b) The spontaneous emission per unit wavelength vs the wavelength. In (b) the measuring aperture was assumed to be 18° wide, collecting all radiation from −9° to 9°. The cavity parameters in both plots are the same as in Fig. 2.

Proper filtering is also important when trying to estimate β from the step height in the output power versus input power curve occurring at threshold [6], unless $\Delta\lambda_{\mathrm{em}}$ is smaller than $\Delta\lambda_{\mathrm{FWHM0}}$. When measuring strictly one mode the step height is equal to $1/\beta$ as will be explained in Sec. V. If proper filtering is not undertaken β will be overestimated by such a measurement, since spontaneous emission belonging to other modes will be included in the measurement. In, e.g., Fig. 2, every density square is 3° by 2.2 nm, that is, the square at 786 nm corresponds to half the cavity mode, which extends from −3° to 3° and from 784.9 to 787.1 nm. If we assume an unfiltered measurement with a $\Delta\lambda_{\mathrm{em}}$ of 20 nm centered around 786 nm, the cavity resonant mode would seem to extend 18° as shown above, and all spontaneous emission between 776 and 796 nm and −9° to +9° would seem to belong to the cavity resonant mode. In this way the resonant mode spontaneous emission would be grossly overestimated. However, above threshold, only the cavity resonant mode will have sufficient optical feedback to lase, so virtually all measured stimulated emission will come from the desired mode, with or without filtering. Therefore the step in the input-power versus output-power curve will be much smaller than $1/\beta$ since the spontaneous emission from many modes measured below threshold is compared with the stimulated emission from one mode above threshold.

III. COMPARISON WITH A DIELECTRIC POST CAVITY

A. Cavity modes

In this section we will compare the behavior of the planar dielectric cavity structure with a three-dimensionally confined structure, namely the dielectric post. The dielectric post cavity is depicted in Fig. 7. A high-refractive-index post ($n \approx 3$) confines the cavity modes tightly in the lateral direction. Integrated Bragg mirrors at each end provides the optical feedback. To solve the dispersion relation for the modes, it is useful to assume that the post has a lossless metal jacket. This will eliminate the (small) evanescent field outside of the dielectric post, and will greatly simplify the dispersion relation. However, the mode solutions will hardly be perturbed at all, since the typically large-refractive-index step between the post and its surroundings will leave very small evanescent field "tails" outside of the post. In other words, the assumed metal jacket will simplify the mathematics without disturbing the physics very much.

The transverse-mode solutions for the cylindrical metal waveguide filled with a dielectric can be found in any standard textbook on microwave engineering. The modes can be described by a set of TE and TM modes, both with

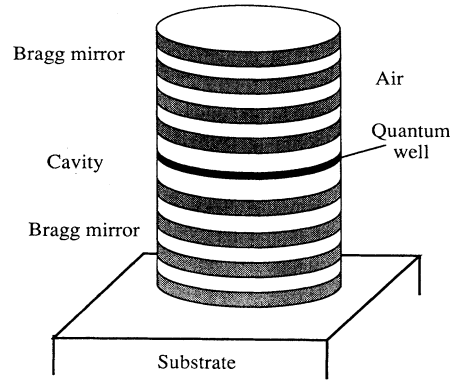

FIG. 7. A schematic drawing of a semiconductor post cavity. The cavity modes are tightly bound to the dielectric post due to the high-refractive-index ratio between the dielectric and the surrounding air.

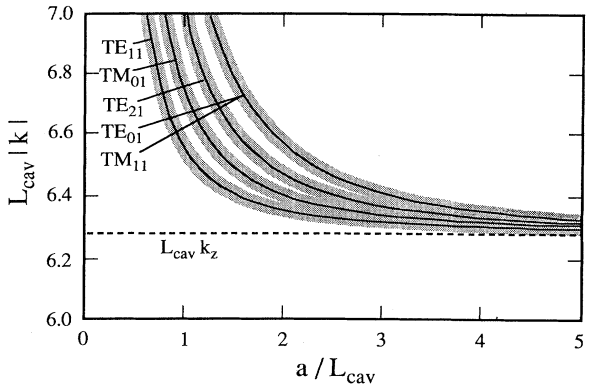

FIG. 8. Normalized dispersion relation for a post laser. The solid thin lines represent the dispersion relation for a post cavity with perfect end reflectors. The grey area represents the "fuzziness" in the dispersion relation introduced by the finite end mirror reflectivity.

a twofold rotational degeneracy (as for the TE modes this is effectively a polarization degeneracy). The dispersion relation for the TE modes is

$$| k |= \left[k_z^2 + \left(\frac{p_{nm}}{a}\right)\right]^{1/2} , \tag{15}$$

where a is the post radius, and p_{nm} is the mth root of the equation $J_n'(p_{nm}) = 0$. J_n here denotes the nth Bessel function of the first kind, and $J_n'(x)$ is the derivative with respect of x of that function. Similarly, the dispersion relation for the TM modes is

$$| k |= \left[k_z^2 + \left(\frac{q_{nm}}{a}\right)\right]^{1/2} , \tag{16}$$

where q_{nm} is the mth root of the equation $J_n(q_{nm}) = 0$.

In an ideal cavity structure, the allowed k-vector z component is given by $k_z = m\pi/L_{\text{cav}}$ where m is an arbitrary positive integer (assuming that the reflection phases of the mirrors are zero or π). However, in a real cavity, the finite mirror reflectivity allows a finite range of k_z's in the mode, as manifested by (6). This spread of k_z will lead to a "fuzziness" of the dispersion relation which has the consequence that at a finite post radius, the mode energies will start to overlap.

Assuming that the gain material in the cavity has a negligibly small gain linewidth $\Delta\lambda_{\text{em}}$, and that its gain is centered at the fundamental TE_{11} mode resonant wavelength, the post radius a must fulfill the relation

$$a \leq \left[\frac{q_{01}^2 - p_{11}^2}{k_z \Delta k_{z,\text{FWHM}}}\right]^{1/2} \tag{17}$$

in order not to make the TM_{01} mode overlap the gain; see Fig. 8. In the figure the spread in k_z is $\Delta k_{z,\text{FWHM}} = 0.05/L_{\text{cav}}$ and consequently the TE_{11} and TM_{01} modes start to overlap when $a_p > 2L_{\text{cav}}$ and the TM_{01} mode overlaps the TE_{11} mode center wavelength when $a_p > 2.8L_{\text{cav}}$. Using (6) the requirement on a_p in order for the resonator to have only one mode solution (more strictly, two rotationally degenerate solutions) can be expressed

$$a \leq \left[\frac{(q_{01}^2 - p_{11}^2)\lambda_{r0} L_{\text{cav}}}{\pi n_{\text{cav}}} \frac{(R_1 R_2)^{1/4}}{1 - (R_1 R_2)^{1/2}}\right]^{1/2}$$
$$= \sqrt{q_{01}^2 - p_{11}^2}\, a_p \approx 1.09 a_p . \tag{18}$$

In the planar cavity the requirement is that the pump radius should be smaller than $\sqrt{2}a_p$. It is obvious that if the gain bandwidth is narrow, the pump radius plays the same role in a planar cavity as the post diameter plays in a post cavity.

In the limit that the post radius becomes very large, specifically when $a \gg a_p$, the two cavity geometries must support the same set of modes for obvious reasons. This seems not to be true since, as explained above, the planar cavity has localized spatial modes, whereas the dielectric post-cavity modes are spread throughout the cavity (global modes). However, in deriving the post-cavity modes, unity mirror reflectivity was assumed. *Only then* will the mode always fill the whole cavity. For finite mirror reflectivities, and hence spread in momentum, Heisenberg's uncertainty principle dictates that the mode size remains finite. The modes in the post can only fill an area πa_p^2. If the post area is larger, localized spatial modes will form. In Sec. IV it will be explained why these localized modes are never observed in a microcavity post laser.

B. Spontaneous-emission coupling factor

The spontaneous-emission coupling coefficient for a dielectric post cavity has already been calculated in Refs. [11,17], and we are not going to repeat the effort. The general characteristics of β are the same for the two cavity geometries. β depends critically on the ratio between $\Delta\lambda_{\text{FWHM0}}$ and $\Delta\lambda_{\text{em}}$ and for obvious reasons it also depends critically on wavelength matching between the cavity resonant mode and the gain.

The difference between the two cavity geometries is subtle, but important. In both cases, to achieve the optimum β, the gain linewidth must be narrower than the

cavity bandwidth. However, in the planar case, the optimum β is determined by the cavity refractive indices. In a typical lattice matched semiconductor system the optimum β is a few percent. In the post case, it is always possible to achieve $\beta \rightarrow 1/2$, provided the gain linewidth is narrow enough. (β cannot approach unity until the rotational mode degeneracy is lifted.) Therefore, it is correct to say that in the dielectric post cavity, the fundamental limit for β is set by the gain bandwidth. This is in complete agreement with the conclusions drawn in [11].

IV. LASING IN PLANAR MICROCAVITIES

A. Review of Schawlow-Townes linewidth formula

The cavity modes of the planar cavity derived in Sec. II B are those of the passive cavity. When the cavity is pumped above threshold, the stimulated emission will preserve the coherence of the spontaneous-emission events, and thus the effective cavity loss will decrease. As can be seen from (14) the cavity mode radius depends on the mirror loss. Above threshold, when there is gain, the mirror loss in (14) should be replaced by effective mirror loss, and the mode will grow in the transverse direction. As the mode grows, the emission lobe will narrow according to (9). This is a consequence of the earlier observation that there is a correspondence between the mode angle and the mode half-width manifested by (4). When the mode linewidth narrows above threshold, as manifested by the Schawlow-Townes linewidth formula, the lobe angle must therefore also narrow.

In the original derivation by Schawlow and Townes, the laser (or rather maser) was viewed as a passive linear filter whose finite Q value determined the filter bandwidth $\Delta\nu$:

$$\Delta\nu = \frac{\nu}{Q} = \frac{\gamma}{2\pi} \quad , \tag{19}$$

where γ is the cavity loss per unit time. Schawlow and Townes realized that this formula should be valid even above threshold, provided that one used the effective cavity loss instead of the cold-cavity loss.

The rate equation for the mean number of photons in the mode p can be expressed as

$$\frac{d}{dt}p = -(\gamma - g)p + \frac{\beta N}{\tau_{sp}} \quad , \tag{20}$$

where g is the material gain per unit time, N is the number of excited atoms (excitons), and τ_{sp} is the spontaneous-emission lifetime. The effective cavity loss for a pumped cavity is seen to be $\gamma - g$. Using the steady-state ($d/dt = 0$) solution of (20) and inserting the effective loss rate into (19), the linewidth can be expressed

$$\Delta\nu = \frac{\beta N}{2\pi\tau_{sp}p} \quad . \tag{21}$$

Assuming a linear gain model $g = g_0(N - N_0)$, where N_0 is the number of excited atoms at material transparency, and using the fact that the stimulated emission at a mean photon number of unity equals the spontaneous emission [4], g_0 can be expressed as $g_0 = \beta N/\tau_{sp}$. Furthermore, using the population inversion factor $n_{sp} = N/(N - N_0)$, and noting that $g \approx \gamma$ above threshold, (21) can be rewritten

$$\Delta\nu = \frac{\gamma n_{sp}}{2\pi p} \quad . \tag{22}$$

Finally, expressing (22) above in emitted power $P = h\nu\gamma p$, and in the cold-cavity bandwidth $\Delta\nu_0 = \gamma/2\pi$, the linewidth can be expressed in an identical way as in the original reference [18]

$$\Delta\nu = \frac{2\pi h\nu(\Delta\nu_0)^2}{P} \quad . \tag{23}$$

This equation is correct below threshold, but gives a result a factor 2 too high above threshold as noted by Lax [19] and others. The factor of 2 is due to that the gain is clamped above threshold, a fact Schawlow and Townes neglected in their linear-filter assumption.

B. Narrowing of divergence angle

As shown in Sec. IV A, the linewidth narrowing of a laser line above threshold can be viewed as the effect of narrow-bandwidth filtering, the decreasing effective loss of the cavity increasing the temporal coherence of the mode, or equivalently the Q value of the filter. In the same manner, the decreasing effective cavity loss will increase the spatial coherence of the mode in a planar cavity, thus making the laser lobe narrower. In contrast to the laser linewidth, there will be a limit to the lobe narrowing set by the pump spot size.

The lobe FWHM of the planar cavity is given by (8). For a high reflectivity cavity, the loss per second can be written $\gamma = -v_g \ln(R_1R_2)/(2L_{cav})$, where v_g is the group velocity of the cavity counterpropagating waves. In defining (8), however, cavity dispersion was neglected, so for the moment we will replace v_g with c_0/n_{cav}. In most cases this is a reasonable approximation. Noting that if $R_1, R_2 \approx 1$, we can replace $2(1 - \sqrt{R_1R_2})$ with $-\ln(R_1R_2)$, the lobe half-width $\Delta\theta_{FWHM0}$ below threshold can be expressed

$$\Delta\theta_{FWHM0} \approx \sqrt{\frac{2\lambda_{r0}n_{cav}^2\gamma}{\pi c_0}} \quad . \tag{24}$$

Using the same arguments as in Sec. IV A, namely that the cavity loss γ in (24) above should be replaced by the effective loss in the laser, one finds that the lobe angle above threshold will be given by

$$\Delta\theta_{FWHM0} \approx \sqrt{\frac{2\lambda_{r0}n_{cav}^2\gamma n_{sp}}{\pi c_0 p}} \quad , \tag{25}$$

where $p \gg 1$. From this equation it appears that the lobe will narrow without bounds as the pumping (and hence p) is increased. This will be true only as long as the effective loss of the mode really decreases with increasing pumping. As long as the mode radius is smaller than the pump spot radius this is true, but in reality the

pumped area will always be finite [Eq. (8) was derived for a cavity with infinite lateral spread], and this will lead to restrictions on the minimum observed lobe angle, as will be discussed in Sec. IV C.

It is also clear that the lobe narrowing will be rather abrupt as a function of pump power, due to the nonlinear behavior of the input versus output relation near the threshold. In a typical planar microcavity laser sample, which has a β of about $1/100$, the mean photon number will jump from unity to about 100 in a very narrow interval around the threshold pump rate [4]. This means that the mode divergence angle will narrow by a factor of 10 (provided that the pump spot radius is at least ten times the cold-cavity mode radius) in the same narrow interval. It will thus be difficult to observe the gradual narrowing of the lobe angle, particularly since the output light has large intensity noise at the threshold. Instead, the lobe will appear to suddenly change divergence angle above threshold.

C. Lateral spread of spatial modes

The mode radius for the cold cavity is given by (14). Again it is appropriate to replace the cold-cavity loss with the effective loss of the active cavity. Doing so we find that the mode radius of the active cavity can be expressed

$$a_p \approx \sqrt{\frac{\lambda_{0r} c_0 p}{\pi n_{\mathrm{cav}} n_{\mathrm{sp}} \gamma}} \quad . \tag{26}$$

However, this equation is only valid as long as $p \gg 1$ and a_p is smaller than the pump spot size. One sees that at the onset of lasing, the mode area will grow proportionally with the output power until the cavity mode fills the entire pump spot. Meanwhile, the power density per unit area remains relatively constant. This can alternatively be viewed as a phase locking of all the spatial mode within the pumped area to a coherent supermode. In absence of cavity imperfections and active material filamentation, a relatively high-power, low-divergence-angle laser could be constructed in this manner.

It is interesting to note that while forming a coupled array of lasers by etching away part of the top mirror in a grid pattern, the coherent supermode far-field pattern of the coupled-laser-array system usually is multilobed, indicating that the individual lasers formed in this way locks out of phase with its neighbors [20]. By avoiding to form individual lasers, the spatial modes of the planar laser will lock in phase, with a narrow divergence, single-lobed emission pattern as a result.

The minimum divergence angle of a planar laser pumped above threshold can now be calculated from (10). If r_{pump} denotes the radius of the pump spot size, the limiting divergence angle will be

$$\Delta\theta_{\mathrm{FWHM0}} \approx \frac{\lambda_{r0}}{2r_{\mathrm{pump}}} \quad . \tag{27}$$

However, if the pump spot size is smaller than the cold-cavity mode radius, then the beam divergence will not narrow appreciably above threshold, because the effective mirror loss over most of the mode area will remain unaffected.

V. EXPERIMENTS

The theory presented in the preceding sections can be compared with experiments we have done with microcavity lasers. These experiments are described in detail elsewhere [6,16]. Here we will give a short overview with emphasis on the comparison of the results with theory. We consider two cases: first, experiments with unmodified planar microcavities [16], which allow a comparison with the prediction for the dependency of β on the linewidth ratio of fluorescence and cavity resonance (Fig. 5). Since the pump spot size for this case is larger than the lasing mode diameter, several transversal modes contribute in the threshold regime as explained in Sec. II B. In order to get a more well-defined situation, a three-dimensional structure was produced by etching, which made single transverse-mode operation possible [6]. A comparison of experimental data with predictions made from the present theory gives a resonable agreement.

A. Planar microcavity

Two planar microcavity structures (A and B) were used for the experimental investigation. Their vertical structure is identical to the model described in Sec. II (Fig. 1). The samples differ essentially in their quantum well thicknesses. Samples A and B have as active media a 70- and a 200-Å single quantum well, respectively. The thicker quantum well of sample B leads to a smaller inhomogeneous broadening and therefore a larger β because of the better coupling of the spontaneous emission to the cavity mode. The quantum well is located in the center of the cavity, at the antinode position of the resonant standing wave, which ensures a good coupling between the field and the active medium. By a variation of the layer thicknesses over the wafer diameter (tapering), different resonant wavelengths result for different positions. The cavity can therefore easily be tuned to the quantum-well emission wavelength by translation of the sample. The cavity features a 80-nm-wide stopband centered around the resonant wavelength, as observed by recording the reflection spectrum of the sample upon illumination with white light. At both ends of the stopband there are highly transmitting windows. The lower wavelength window was used for coupling the appropriately tuned pump light, obtained from a Ti:sapphire laser, into the cavity, thereby reducing the reflection losses to 15%.

For the measurements the microcavity was placed in a liquid-helium dewar and cooled to 4 K. This reduced the fluorescence linewidth by more than an order of magnitude, and contributed to optimizing the coupling ratio between cavity and fluorescence linewidth. In structure B the resulting emission linewidth was 2.5 nm, which is wider than the cavity resonance width. For the narrower quantum well in structure A, a broader linewidth of 5.3 nm was measured, which is due to increased inhomogeneous broadening and leads to a somewhat reduced β. The photon energy at the pump wavelength (740 nm for

sample B) is below the band-gap energy of the layers constituting the mirrors, so no serious absorption occurs. The incident beam is focused to a spot of 25 μm diameter and the spatially filtered outcoming light is analyzed using a monochromator, providing a wavelength selectivity of the order of the cavity linewidth.

The result of an input versus output-power measurement of the planar structure B is shown in Fig. 9. For the present purpose, we are mainly interested in the height of the step at the threshold, as it appears in the double logarithmic plot, since it allows estimating the spontaneous-emission factor of the cavity. This is because in the absence of nonradiative processes, the quantum efficiency above threshold is close to unity, and below threshold, by the definition of the spontaneous-emission coefficient, it is equal to β. Fitting the theoretical input-output curve as obtained by a rate-equation model [4] to the data, we obtain a β value of 10^{-2} for sample B and 6×10^{-3} for sample A. The latter value is somewhat lower, as one should expect from the degraded atom-cavity coupling due to the larger fluorescence linewidth, and comparison of the experimental points with the theoretical curve in Fig. 5 shows a good agreement. In order to determine the number of transverse modes being excited by the pump laser, a measurement of the divergence angle of the fluorescence below threshold was made. The $1/e^2$ lobe angle of 8° corresponding to a $\Delta\theta_{\mathrm{FWHM0}}$ of about 5.2°. Using (8) and (14), the cavity mode radius is inferred to be about 3.8 μm. This is considerably smaller than the pump spot size of 25 μm. Therefore at threshold several independent lasers can start oscillating in the pumped area, which is equivalent to multiple-transverse-mode operation. Thus there is still the possibility of a systematic error in the estimation of β in spite of the filtering, since the area contributing to the measured photon fluxes above and below threshold may be different as explained in Sec. IV. A true single-mode measurement, as presented below, is safer in this respect.

An independent way to determine β is to measure the cold-cavity linewidth and then use Fig. 5. A measurement with a scanning Fabry-Pérot interferometer yielded a $\Delta\lambda_{\mathrm{FWHM0}}$ of 0.43 nm which leads to estimated β values of 3.5×10^{-3} and 8.3×10^{-3} for samples B and A, respectively. This is in quite good agreement with the estimate based on the input versus output power measurement. However, $\Delta\lambda_{\mathrm{FWHM0}}$ and thus β can also be estimated indirectly from the mode divergence angle through (7) and (8). The resulting figures are $\Delta\lambda_{\mathrm{FWHM0}} = 0.13$ nm and $\beta = 1.3 \times 10^{-3}$ for sample A and 2.8×10^{-3} for sample B. This very indirect method of estimating β leads to worse agreement with the estimate based on the input versus output-power measurement. However, it leads us to conclude that neither the mode radius nor β of our samples are known to better than a factor of 2.

B. Etched cavity

In order to make sure that no higher-order transverse modes participate when going from below to above threshold, the pump spot size was reduced, but this turned out to have no effect, possibly because of the diffusion of carriers. However, the single-mode operation could be achieved by altering the cavity geometry: An array of three-dimensional microlasers was obtained by chemical wet etching of sample B, yielding circular mesalike structures of various diameters (Fig. 10). The etch depth was chosen such as to remove the upper mirror, the active region, and half of the lower mirror in the unmasked parts. The resulting microlasers have a small top-mirror diameter, which acts like a pinhole for the cavity field, leading to increased losses for non-TEM_{00} modes and therefore encouraging single-mode operation. On the other hand, the diameter at the quantum well is 4–5 μm larger. This reduces losses due to carriers diffusing to the etched surface and recombining there. Although the etched sample have three-dimensional microlaser structures, they must still be considered as planar microcavities, since the diameters involved are equal or larger than the planar-cavity-mode diameter. In this regime waveguide effects are not important.

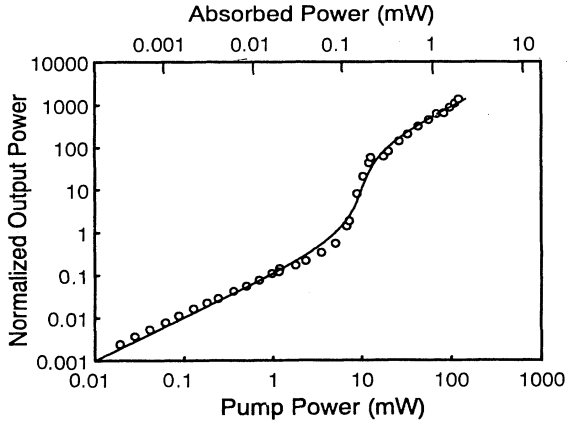

FIG. 9. Output power vs input power for the planar sample B ($\lambda = 810$ nm). The solid line is the theoretical curve. The vertical scale is normalized to the theoretical number of photons in the lasing mode, being unity at threshold.

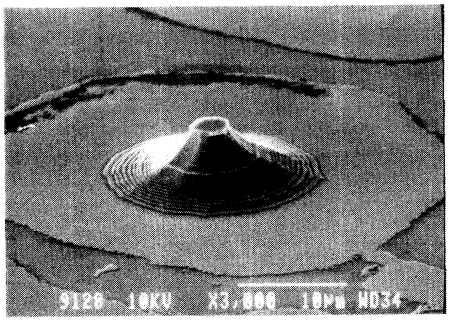

FIG. 10. Scanning electron microscopic picture of one of the microlasers obtained by etching the planar sample B (diameter 3.4 μm). The top surface acts as a pinhole, increasing the losses for higher-order transverse modes and thereby leading to single-mode operation. The broad band in the middle of the structure is the one-wavelength spacer containing the quantum well. The larger quantum-well diameter reduces the surface recombination.

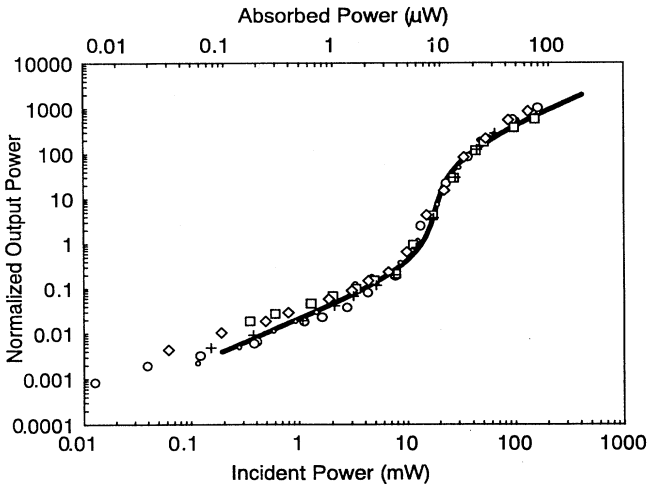

FIG. 11. Superposition of several input-output curves obtained for a 3.4-μm microlaser. The threshold powers of the individual curves differ by $\pm 40\%$.

The sample was pumped with a spot diameter of 20 μm, and showed lasing at 805 nm. The input versus output curve for a microlaser with top mirror diameter of 3.4 μm is shown in Fig. 11. Fitting the theoretical curve yields a β factor of 9×10^{-3}. The threshold as defined by the one-photon condition [4] is $P_{\text{thr}}= 6.7$ μW absorbed power, corresponding to 4-μA current for the case of electrical pumping. This should be compared to the threshold current of commercial diode lasers, which is of the order of 10 mA. Thus several orders of magnitude reduction of threshold is indeed possible using microcavity lasers.

Data obtained for different microlaser diameters are shown in Fig. 12. The increased pump power needed to bring the larger structures to the threshold is apparently consumed for increasing the number of independent oscillators. As predicted in Sec. II B, the line slope in the doubly logarithmic plot is approximately 2, so the required pump-power density is roughly equal for all the lasers on the line. Conversely, the enhanced power density required for the 3.4-μm laser confirms that this structure actually lases single mode.

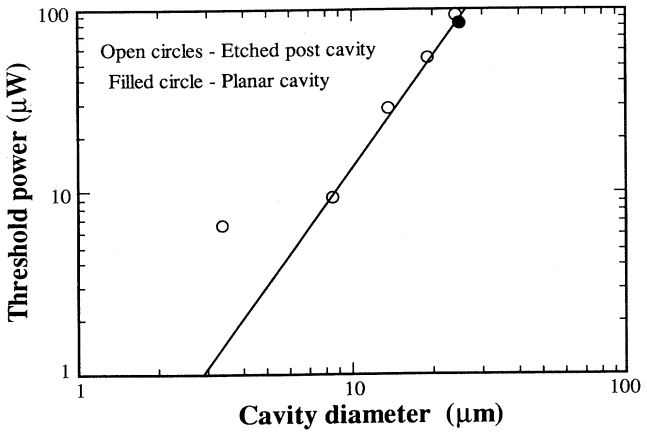

FIG. 12. Absorbed pump power at threshold vs cavity top mirror diameter. The filled circle pertains to a planar (nonetched) laser pumped with a 25-μm-diam beam. The fitted curve has a slope of 2.1.

Having a single-mode oscillator allows us to make a quantitative comparison between experiment and theory. The expected threshold power can be calculated from

$$P_{\text{thr}} = \frac{h\nu\gamma}{2\beta} \quad . \tag{28}$$

Using the values of β estimated from the linewidth measurement for the planar sample, and using the relation $\gamma = 2\pi c_0 \Delta\lambda_{\text{FWHM0}}/\lambda_0^2$, we get P_{thr}=18 μW. Thus, the observed values of β and P_{thr} are in reasonable agreement with the theoretical expectation.

VI. CONCLUSION

The spontaneous-emission pattern and the spontaneous-emission coupling coefficient β of planar semiconductor microcavities have been computed and measured experimentally. Reasonable agreement has been found between experiments and theory. The planar structure is simple to fabricate, but the ease of fabrication is bought at the cost of limited achievable β, the latter being determined by the refractive indices in the Bragg mirrors and the cavity. It was demonstrated that in order to maximize β, the gain linewidth of the active material must be smaller than the cold-cavity linewidth. For a typical single quantum-well microcavity laser the gain linewidth must be smaller than 1 nm to meet this requirement. It was shown that, in spite of having no lateral confinement, well-defined, circularly symmetric, spatially localized modes will form in the planar cavity. In order to have a single-mode (or rather a two-mode) device, the pump spot size should be smaller than the mode area. It was also pointed out that in order to experimentally characterize a planar cavity, it is in general important to filter the measured light, both spatially and in wavelength. The reason is the peculiar cavity resonance of the planar cavity, which may extend far outside the cavity mode, both in wavelength and in angle. Above threshold it is expected that the resonant-mode radius will grow; it will eventually fill the whole pumped area. The lateral growth of the mode will be accompanied by a narrowing of the far-field lobe angle. It was shown that this behavior is analogous to the linewidth narrowing of laser light with increasing pumping. The planar cavity was compared to a dielectric post cavity. It was shown that in many respects they are similar, the post radius playing the same role as the pump spot size in the planar-cavity case. However, an important difference is that the β of the post cavity is in general not limited by the cavity refractive index, but rather on the active-material gain linewidth.

ACKNOWLEDGMENTS

One of the authors (G.B.) would like to thank NTT for kindly inviting him to visit. G.B. also acknowledges generous assistance from the National Board for Industrial and Technical Development, Sweden (NUTEK).

[1] F. De Martini and G. R. Jacobovitz, Phys. Rev. Lett. **60**, 1711 (1988).
[2] H. Yokoyama and S. D. Brorson, J. Appl. Phys. **66**, 4801 (1989).
[3] Y. Yamamoto, S. Machida, and G. Björk, Phys. Rev. A **44**, 657 (1991).
[4] G. Björk and Y. Yamamoto, IEEE Quantum Electron. **QE-27**, 2386 (1991).
[5] S. L. McCall *et al.*, Appl. Phys. Lett. **60**, 289 (1992).
[6] H. Heitmann *et al.*, in *Quantum Electronics & Laser Science,* 1992 Technical Digest Series, Vol. 13, QPD11 (Optical Society of America, Washington, D.C., 1992); H. Heitmann, Y. Kadota, T. Kawakami, and Y. Yamamoto (unpublished).
[7] J. L. Jewell, J. P. Harbison, A. Scherer, Y. H. Lee, and L. T. Florez, IEEE J. Quantum. Electron. **QE-27**, 1332 (1991).
[8] K. H. Lin and W. F. Hsieh, Opt. Lett. **16**, 1608 (1991).
[9] F. M. Matinaga *et al.,* Appl. Phys. Lett. **62**, 443 (1993).
[10] G. Björk, Y. Yamamoto, S. Machida, and K. Igeta, Phys. Rev. A **44**, 669 (1991).
[11] T. Baba, T. Hamano, F. Koyama, and K. Iga, IEEE Quantum Electron. **QE-27**, 1347 (1991).
[12] Y. Yamamoto, S. Machida, Y. Horikoshi, K. Igeta, and G. Björk, Opt. Commun. **80**, 337 (1991).
[13] K. Ujihara, Jpn. J. Appl. Phys. **30**, 901 (1991).
[14] F. De Martini, M. Marrocco, and D. Murra, Phys. Rev. Lett. **65**, 1853 (1990).
[15] E. Yablonovitch *et al.*, Opt. Quantum Electron. **24**, S273 (1992).
[16] R. J. Horowicz, H. Heitmann, Y. Kadota, and Y. Yamamoto, Appl. Phys. Lett. **61**, 393 (1992).
[17] T. Baba, T. Hamano, F. Koyama, and K. Iga, IEEE Quantum Electron. **QE-28**, 1310 (1992).
[18] A. L. Schawlow and C. H. Townes, Phys. Rev. **112**, 1940 (1958).
[19] M. Lax, in, *Physics of Quantum Electronics*, edited by P. L. Kelley, B. Lax, and P. E. Tannenwald (McGraw-Hill, New York, 1966).
[20] M. Orenstein *et al.*, Appl. Phys. Lett. **58**, 804 (1991).

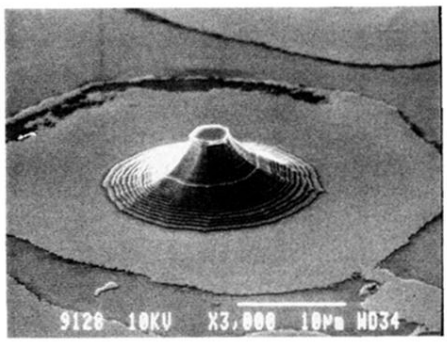

FIG. 10. Scanning electron microscopic picture of one of the microlasers obtained by etching the planar sample B (diameter 3.4 μm). The top surface acts as a pinhole, increasing the losses for higher-order transverse modes and thereby leading to single-mode operation. The broad band in the middle of the structure is the one-wavelength spacer containing the quantum well. The larger quantum-well diameter reduces the surface recombination.

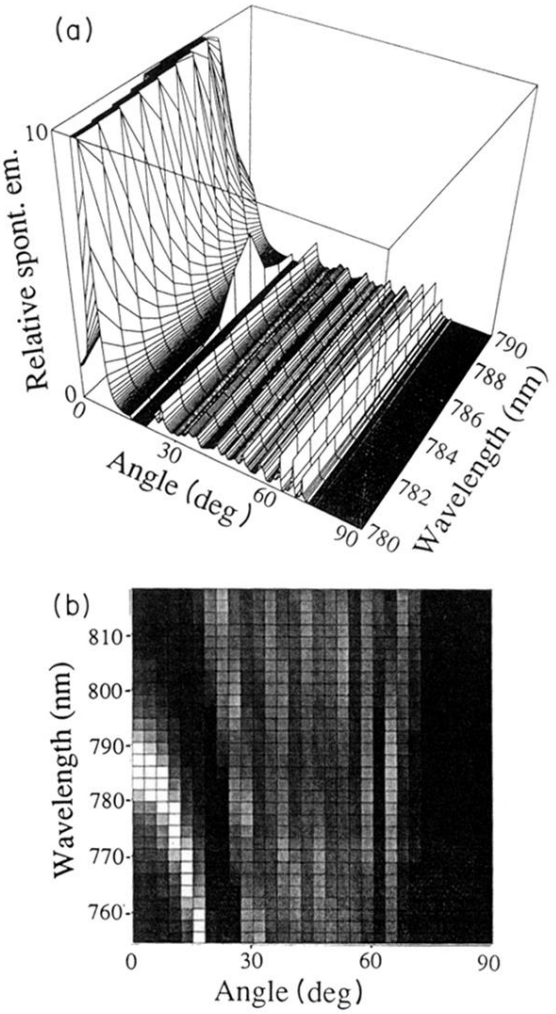

FIG. 2. Computed spontaneous emission per unit solid angle and unit wavelength (arbitrary units) vs emission wavelength and propagation angle in the cavity. The z axis in (a) has been truncated at about one-fourth of the spontaneous-emission maximum to resolve details in the passband. In (b) a density plot over the spontaneous-emission intensity has been drawn. White represents values > 2.5 in. [cf. (a)], black represents zero. It can be seen that the spontaneous emission has its maxima on a half parabola on the lower wavelength side. The jaggedness in both figures is due to the limited plot resolution.